ACS OMEGA

Article

Cite This: ACS Omega 2019, 4, 17850−17856

http://pubs.acs.org/journal/acsodf

Polyamine-Modified Gold Nanoparticles Readily Adsorb on Cell Membranes for Bioimaging

Xiang-Fu Du, Bing-Jie Zhu, Zhong-Chao Cai, Chaojie Wang, and Mei-Xia Zhao*

Key Laboratory of Natural Medicine and Immune Engineering, Henan University, Jinming Road, Kaifeng 475004, China

Supporting Information

ABSTRACT: The surface modification of nanoparticles (NPs) can enhance cellular and intracellular targeting. A new type of polyamine-modified gold NPs (AuNPs) are designed and synthesized, which can be selectively absorbed onto the cell membrane. AuNPs with an average diameter of 4.0 nm were prepared and modified with polyamine (R-4C) through amidation. In order to detect the distribution of NPs within cells by fluorescence imaging, AuNP@MPA-R-4C was functionalized with fluorescein isothiocyanate (FITC). The fluorescence-labled NPs AuNP@MPA-R-4C-FITC demonstrated minimal cytotoxicity in several cell lines. Both confocal laser scanning microscopy and transmission electron microscopy demonstrated that AuNP@MPA-R-4C-FITC was distributed on the cell membrane. Compared with the free organic dye, the modified AuNPs showed significantly increased accumulation on the cell membrane after treatment for only 10 min. These results suggested that AuNP@MPA-R-4C-FITC can be used as a bioprobe targeting the cell membrane for various biological applications.

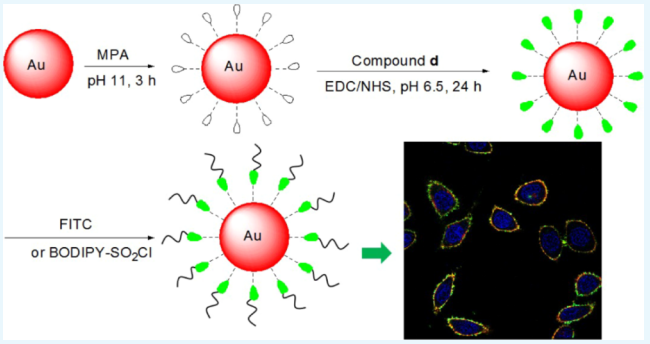

INTRODUCTION

The cell membrane has many important physiological functions.[1,2] It stabilizes and controls the intracellular environment by selectively permitting the entry of certain biomolecules while excluding others. Cell membranes facilitate this through several mechanisms, including passive diffusion, direct uptake, endocytosis, and exocytosis.[3] The cell membrane also plays an important role in cell recognition, signal transmission, cellulose synthesis, microfibril assembly, and others.[4−8]

Gold nanoparticles (AuNPs) are currently one of the most widely studied nanomaterials because of their unique optical properties, high chemical stability, and biocompatibility.[9−13] It has broad potential for application in nanoelectronics, nanophotonics, catalysis, sensors, biomarkers, and many other areas.[14−18] Notably, AuNPs have a large surface area and can be used as a carrier for fluorescent dyes.[19,20] NPs have often been used in fluorescence immunoassay to improve the detection sensitivity.[21] As fluorescent probes, AuNPs can control cell function, regulate gene expression, and detect analytes in the cells.[22−24] Therefore, improving functionalized AuNPs has become an area of interest in the development of fluorescent probes. Amino acids are the basic compositional unit of proteins, and are also essential nutrients in animal diets.[25,26] Amino acid derivatives demonstrate significant biological function and can be designed to interact with intracellular targets.[27,28] Despite of the many advances in the development of fluorescent probes, a fundamental issue remaining to be addressed is the cytotoxicity and target specificity.

In this context, AuNPs functionalized with amino acid derivatives for biological targeting properties were synthesized (Scheme 1a,b). The amino acids included L-tryptophan (L-Trp), L-lysine (L-Lys), L-cysteine (L-Cys), and L-glutamic (L-Glu). The AuNPs were first modified with 3-mercaptopropionic acid (MPA) to form a self-assembled monolayer and were subsequently conjugated with R-4C through the formation of amide bonds between the terminal amines on R-4C and the terminal carboxylic acid on the particles. FITC is a versatile agent used for cell imaging by confocal microscopy. Although AuNPs are known to be a very efficient fluorescence quencher,[29] the attachment of FITC through the R-4C spacer did show significant emission intensity. In order to detect the distribution of NPs in cells by fluorescence imaging, AuNP@MPA-R-4C was functionalized with FITC by amidation (Scheme 1c). MTT assay demonstrated that these modified AuNPs did not cause cytotoxicity in several kinds of cells. Both confocal laser scanning microscopy (CLSM) and transmission electron microscopy (TEM) demonstrated that the modified AuNPs were mainly distributed on the cell membrane. The modified AuNPs can enter the cell membrane after incubating for just 10 min and can persist for at least 6 h on the cell membrane. These results suggest that surface modification can

Received: August 13, 2019
Accepted: October 9, 2019
Published: October 17, 2019

DOI: 10.1021/acsomega.9b02579
ACS Omega 2019, 4, 17850−17856

Scheme 1. Schematic Illustration of the Synthesis of AuNP@MPA-R-4C-X[a]

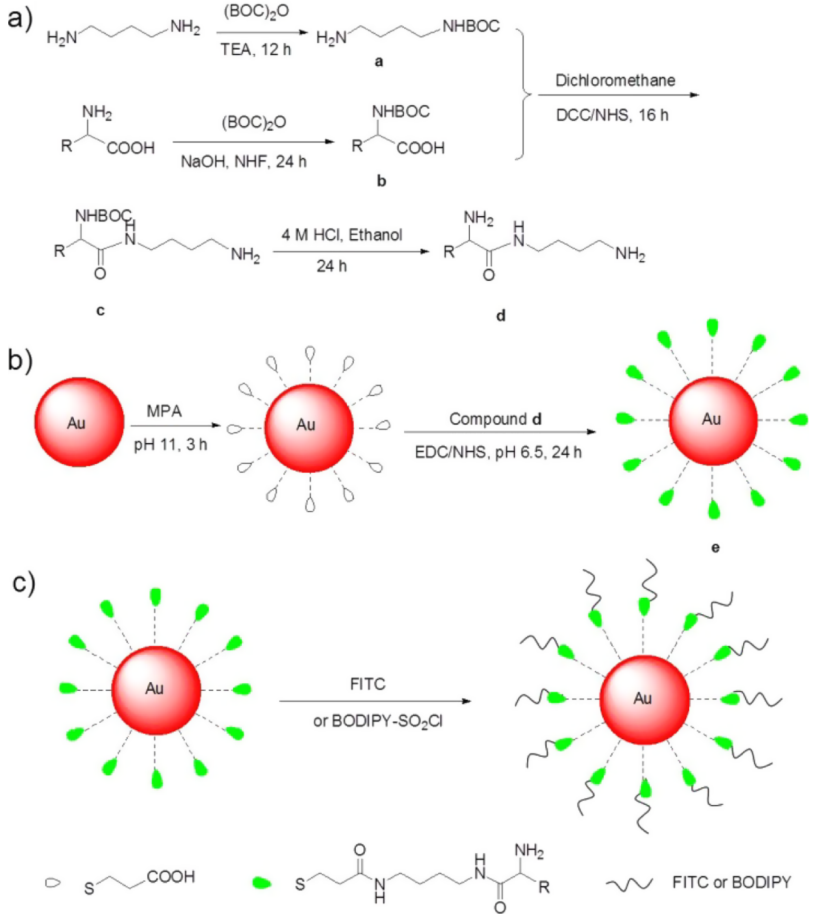

[a](a) Synthesis of R-4C, (b) synthesis of AuNP@MPA-R-4C, (c) synthesis of AuNP@MPA-R-4C-X. (R = L-tryptophan (L-Trp), L-lysine (L-Lys), L-cysteine (L-Cys), and L-glutamic (L-Glu) residues; X = FITC or BODIPY).

enhance the stability and improve the biocompatibility of AuNPs. Moreover, these modified AuNPs can selectively enter the cell membrane to facilitate the targeting of a fluorescent probe.

RESULTS AND DISCUSSION

Preparation and Characterization of AuNPs. The citrate-stabilized AuNP@MPA was prepared by sodium borohydride reduction of tetrachloroauric(III) acid solution in the presence of sodium citrate. The morphology of AuNP@MPA was characterized by TEM (Figure S1a, Supporting Information). The results showed that these NPs were uniformly dispersed with a spherical shape, and had an average diameter of 4.5 nm. AuNP@MPA-R-4C-FITC was then prepared (Scheme 1). Amino acids can be divided into several groups based on its polarity, including nonpolar, polar without charge, polar with positive charge, and polar with negative charge.[30] Thus, we selected representative amino acids from each group, including L-Trp, L-Cys, L-Lys, and L-Glu acid. First, AuNP@MPA was conjugated with R-4C through amidation between the terminal amines on R-4C and the terminal carboxylic acid groups on the particles. The biocompatible R-4C not only serves as a coating to increase protein adsorption and specific macrophage uptake, but also serves as a linking agent providing terminal functional groups for the conjugation of ligands, such as FITC and BODIPY. In order to detect the distribution of AuNPs in cells by fluorescence imaging, AuNP@MPA-R-4C was further functionalized with FITC through amidation.[31] AuNPs were characterized by TEM and dynamic light scattering (DLS) for particle size and size distribution. TEM results showed that the size distribution of AuNP@MPA-R-4C-FITC was similar to that of the AuNP@MPA particles and had an average diameter of 6.0, 6.2, 5.7, and 5.7 nm, respectively (Figure S1, Supporting Information). Namely, the size increased by 1−2 nm for AuNPs because of the coating with polymer R-4C-FITC. Moreover, the corresponding hydrodynamic-diameter distributions of the AuNPs in water measured by DLS are shown in Figure S2 in Supporting Information, giving average hydrodynamic diameters of 5.0, 6.7, 9.1, 7.1, and 7.2 nm, respectively. Moreover, DLS analysis indicated that there were some aggregations of AuNPs. These results are also in agreement with TEM observation. These data indicated that the morphology of AuNPs was unaffected by the added polymer R-4C-FITC. AuNP@MPA-R-4C-FITC NPs demonstrated little aggregation, probably because of the interactions between the functional groups on the surface of the NPs.[32]

The representative UV−vis absorption spectra of AuNP@MPA and AuNP@MPA-Lys-4C-FITC NPs (Figure S3, Supporting Information) showed that the UV−vis absorption spectra of AuNP@MPA-Lys-4C-FITC exhibited a new absorption band at 530 nm compared with that of AuNP@

DOI: 10.1021/acsomega.9b02579
ACS Omega 2019, 4, 17850−17856

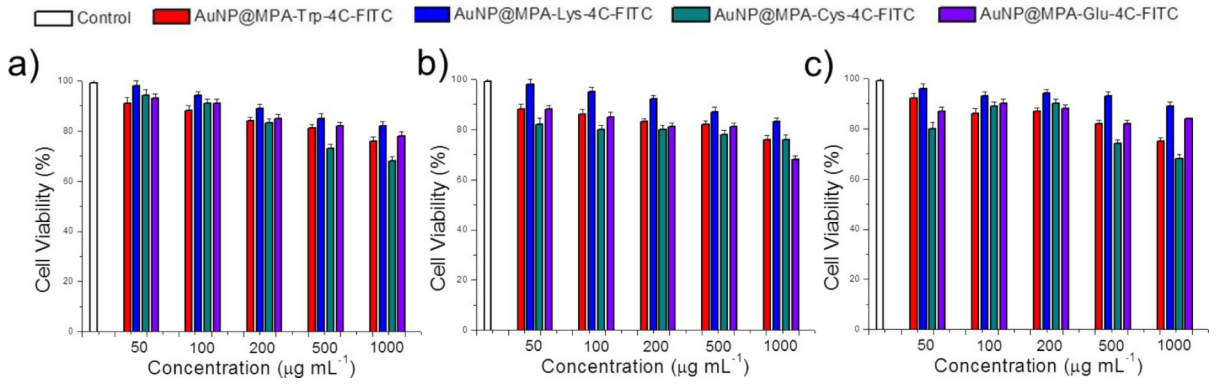

Figure 1. Cell viability of Au@MPA-Trp-4C-FITC, Au@MPA-Lys-4C-FITC, Au@MPA-Cys-4C-FITC, and Au@MPA-Glu-4C-FITC with (a) HepG2 cells, (b) MCF-7 cells, and (c) QSG-7701 cells. Cells were incubated with samples at different concentrations at 37 °C for 48 h.

MPA, which was absorbed at 343 nm. There was no significant change in the position or the width of absorbance bands from AuNP@MPA, suggesting that Lys-4C-FITC derivatives were successfully incorporated into AuNP@MPA NPs.

The AuNPs were further characterized by fluorescence spectroscopy. The emission spectra of AuNP@MPA and AuNP@MPA-R-4C-FITC (Figures S4 and Figure S5, Supporting Information) showed that the fluorescence intensity at 561 nm was increased in AuNP@MPA-Trp-4C or AuNP@MPA-Lys-4C; however, the fluorescence intensity at 516 nm decreased upon FITC conjugation. This change was attributed to the fluorescence resonance energy transfer (FRET) with FITC as the donor and AuNP@MPA-Trp-4C or AuNP@MPA-Lys-4C as the acceptor. This is consistent with the overlap between the absorption spectra of the later with the fluorescence spectrum of the former. FRET is possible only when the two species are in close physical proximity, typically within nanometers of each other. Therefore, the observation of FRET in this case further indicates complex formation between these two oppositely charged species.

Cell Cytotoxicity. To explore the cell toxicity of AuNPs, HepG2, QSG-7701, and MCF-7 cells were treated with AuNPs at different concentrations for 48 h according to the standard methylthiazole tetrazolium (MTT) assay. The cell viabilities of these AuNPs are shown in Figure 1. Obviously, AuNP@MPA-R-4C-FITC showed lower toxicity in the three kinds of cells in our study. These results suggested that AuNP@MPA-R-4C-FITC caused less damage to normal cells and cancer cells. Especially, the cytotoxicity of AuNP@MPA-Lys-4C-FITC with positive charge was lower than other AuNPs. The surface charge of the lysine residue-modified APs is highly positive, which allows interaction with a negatively charged cell surface. Maybe, the lysine residue with more positive charge can significantly affect the minimal cytotoxicity.[33]

Intracellular Uptake of AuNPs. Because AuNP@MPA-Lys-4C-FITC demonstrated good optical properties and minimal cytotoxicity, its specific binding to the surface of living cells was investigated in HepG2 cells. AuNP@MPA-R-4C-FITC is sufficiently fluorescent and its intracellular behavior is visible by CLSM. AuNP@MPA-Lys-4C-FITC nanoconjugates showed considerably stable fluorescence when excited at 488 nm. To study the intracellular uptake of AuNPs, HepG2, MCF-7, and QSG-7701 cells were incubated with AuNP@MPA-Lys-4C-FITC for 10 min and the cellular fluorescence signal was imaged using CLSM. Figure 2 shows the fluorescence images of HepG2, MCF-7, and QSG-7701

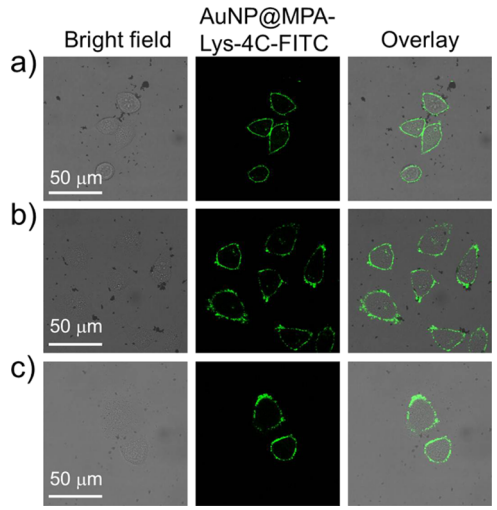

Figure 2. Confocal images of (a) HepG2, (b) QSG-7701, and (c) MCF-7 cells treated with AuNP@MPA-Lys-4C-FITC for 10 min at 37 °C.

cells incubated with AuNP@MPA-Lys-4C-FITC at a concentration of 500 μg/mL. We observed that AuNP@MPA-Lys-4C-FITC was uptaken by cells. These results demonstrated that AuNP@MPA-R-4C-FITC can permeate the cell membrane and enter the cells.

Moreover, we studied the time-dependence and concentration-dependence of the cellular uptake of AuNP@MPA-R-4C-FITC. Figure 3 shows the fluorescence images of HepG2 with AuNP@MPA-Lys-4C-FITC at different concentrations. We found that the fluorescence intensity increased with increasing concentration. Also Figure 4 shows the fluorescence images of HepG2 treated with AuNP@MPA-Lys-4C-FITC for different incubation times. We can observe that the fluorescence intensity decreased as the incubation time increased. AuNP@MPA-Lys-4C-FITC was found to enter the cell quickly within 10 min (Figure 4a). However, after 6 h incubation, the signal decreased significantly in the green channel (Figure 4e). Thus, the fluorescence intensity of AuNP@MPA-R-4C-FITC-treated cells varied with different sample concentrations and incubation times. The fluorescence of the NPs faded over time mainly because of the exocytosis of AuNPs into cells. Some NPs disintegrated in the endolysosomal compartments of HepG2 cells, followed by slow metabolism.[34,35]

DOI: 10.1021/acsomega.9b02579
ACS Omega 2019, 4, 17850−17856

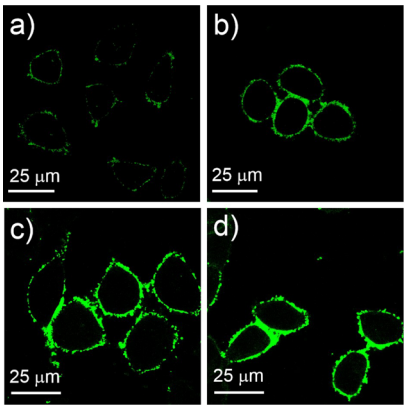

Figure 3. Confocal images of HepG2 cells treated with AuNP@MPA-Lys-4C-FITC for 10 min at 37 °C with different concentrations: (a) 100, (b) 500, (c) 1000, and (d) 2000 μg/mL.

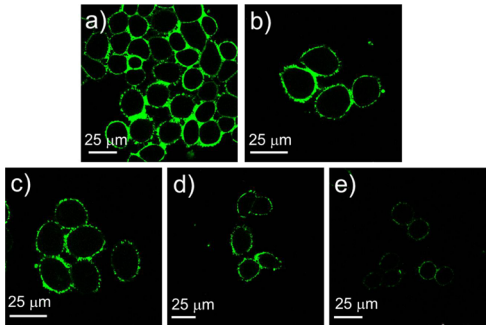

Figure 4. Confocal images of HepG2 cells treated with AuNP@MPA-Lys-4C-FITC (500 μg/mL) at 37 °C in the medium at different time: (a) 10 min, (b) 30 min, (c) 1 h, (d) 3 h, and (e) 6 h.

Selective Localization of the AuNPs in Vitro. The accumulation of these AuNPs within subcellular compartments was of particular importance. To confirm the selective localization of the AuNPs in vitro, HepG2 cells were incubated with AuNP@MPA-Lys-4C-FITC. After incubation for 10 min, the cells were washed. In vitro intracellular colocalization of AuNP@MPA-Lys-4C-FITC with WGA−Alexa Flour 594 (cytomembrane dye) in HepG2 cells was investigated using CLSM. As shown in Figure 5, AuNP@MPA-Lys-4C-FITC had

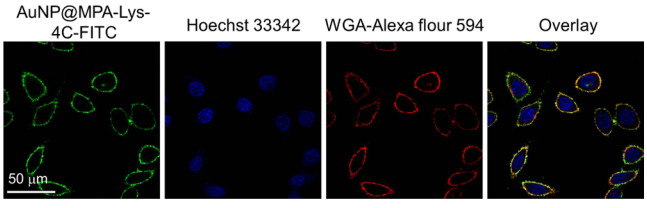

Figure 5. Confocal microscopy of HepG2 cells incubated with 500 μg/mL AuNP@MPA-Lys-4C-FITC (green) for 10 min at 37 °C. Cells were stained with Hoechst (blue) for the nucleus, WGA−Alexa Flour 594 for cytomembrane (red).

complete colocalization with cytomembrane dye in HepG2 cells. In order to confirm that the fluorescent dye did not affect the accumulation of NPs within the cell membrane, another dye BODIPY was combined with AuNP@MPA-R-4C. As shown in Figure 6, AuNP@MPA-Lys-4C-BODIPY also had complete colocalization with cytomembrane dye in HepG2 cells. Evaluation of the staining patterns and colocalization

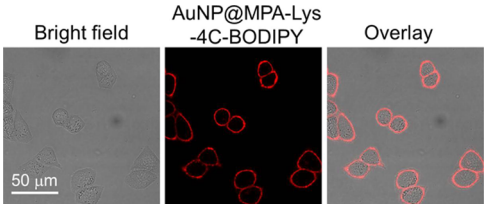

Figure 6. Confocal images of HepG2 cells treated with AuNP@MPA-Lys-4C-BODIPY (500 μg/mL) for 10 min at 37 °C.

revealed that the AuNPs can remain intact after uptake and can be predominantly confined within the cytomembrane.

In contrast, HepG2 cells treated with free FITC under the same conditions exhibited a high level of fluorescence in cell nucleus (Figure S6, Supporting Information). Importantly, the fluorescence of the modified AuNPs can be observed only in the cell membrane areas, whereas FITC fluorescence was detected in the nucleus, indicating that the modified AuNPs easily penetrated into the cell membrane instead of the nucleus. The efficient internalization of the AuNPs demonstrated that Lys-4C facilitated the specific intracellular uptake, which was driven mainly by endocytosis.[36] Accumulation of AuNPs within the cytomembrane suggested that the uptake was dominant. This evidence indicated that nearly all of the endocytosed AuNPs were transported inside the cytomembrane without being released into the cytoplasm or nucleus.

Furthermore, the localization of modified AuNPs in HepG2 cells was observed by TEM. As shown in Figure 7, the AuNP@

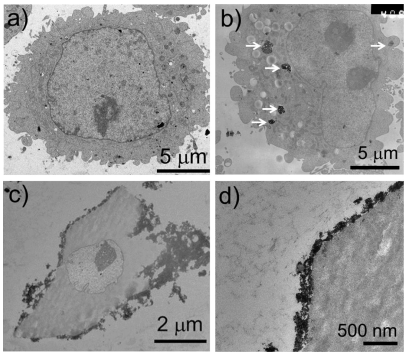

Figure 7. Representative TEM images of HepG2 cells: (a) control, (b) treated with AuNP@MPA (500 μg/mL), and (c,d) treated with AuNP@MPA-Lys-4C-FITC (500 μg/mL) for 10 min.

MPA NPs were scattered in the cytoplasm; however, the modified AuNPs were not scattered in the cytoplasm, but clustered and attached to the cytomembrane. This was likely because of electrostatic interactions between the positively charged AuNPs and the negatively charged membranes. All these results confirm that AuNPs can be leveraged as a platform for cytomembrane targeted probes in bioimaging. The low toxicity of AuNPs toward cells further confirms that AuNPs are a promising fluorescent probe for in vitro imaging of cellular processes.[37]

CONCLUSIONS

In conclusion, we present the modification of 4 nm AuNPs using MPA, R-4C, FITC, and BODIPY. The multiple amine groups on the particle surface allow conjugation onto the particles with a variety of molecules through the formation of amide bonds under mild conditions. This property makes these

DOI: 10.1021/acsomega.9b02579
ACS Omega 2019, 4, 17850−17856

particles ideal candidates for the enhancement of targeting. Both CLSM and TEM demonstrate that AuNP@MPA-Lys-4C-FITC NPs are distributed on the cell membrane. Thus, AuNP@MPA-R-4C-FITC can be used as a bioprobe swallowed by the cell membrane for studying biological processes.

EXPERIMENTAL SECTION

Chemicals and Materials. 1,4-Butanediamine, di-*tert*-butyl dicarbonate ($(BOC)_2O$), pyrrole, 2-pyrrolecarbaldehyde, boron fluoride etherate ($BF_3{\cdot}O(Et)_2$), sodium carbonate (Na_2CO_3), sodium sulfate (Na_2SO_4), sodium hydroxide (NaOH), and triethylamine (Et_3N) were purchased from Alfa Aesar company. L-Tryptophan (L-Trp), L-cysteine (L-Cys), L-lysine (L-Lys), L-glutamic (L-Glu) acid, sodium borohydride ($NaBH_4$), MPA, trisodium citrate dihydrate, tetrahydrofuran (THF), phosphorus oxychloride ($POCl_3$), cyanuric chloride (TCT), dimethyl sulfoxide (DMSO), *N*,*N*′-dicyclohexylcarbodiimide (DCC), carbodiimide (EDC), *N*-hydroxy succinimide (NHS), 2-(*N*-morpholino) ethanesulfonic acid (MES), and fluorescein isothiocyanate (FITC) were purchased from Shanghai Reagent Company. Fetal bovine serum (FBS) and RPMI-1640 media were from Invitrogen Corporation. All organic solvents were purchased from EM Sciences. MCF-7 (human breast cancer cells), HepG2 (human hepatocellular liver carcinoma cells), and QSG-7701 (human normal hepatocyte) cells were purchased from the Shanghai Institute for Biological Sciences, Chinese Academy of Sciences (Shanghai, China).

Apparatus. UV−vis absorption spectra were acquired with a Varian Cary 300 BIO UV−vis spectrophotometer equipped with a temperature controller (±0.1 K). The fluorescence spectra were recorded by using a Cary Eclipse fluorescence spectrophotometer (American, Agilent, Co.). The transmission electron microscopy (TEM) images of the products were taken on a JEOL JEM-200CX transmission electron microscope, employing an accelerating voltage of 200 kV. DLS measurements were detected on a BI-200SM laser light scattering system (Brookhaven Instruments Corporation).

Synthesis of AuNPs@MPA. Citrate-capped AuNPs with an average size of 4.5 nm were synthesized following the method reported by Turkevich et al.[38] In detail, 2 mL of 15 mM chloroauric acid solution ($HAuCl_4$) and 773 μL of 38.8 mM sodium citrate solution were added to 30 mL of deionized H_2O and kept stirring. Then 3 mL of freshly prepared 0.1 M $NaBH_4$ was added. After reacting for 2 h, the solution changed from colorless to light orange. Then 3 mL 0.01 M MPA (in anhydrous ethanol) solution was added to the above solution at pH 11, and kept reacting for another 2 h.

General Procedure for the Synthesis of AuNPs@MPA-R-4C. *Synthesis of Compound* ***a***. A mixture of 1,4-butyl diamine (2.2 g, 25 mmol), 15 mL 10% of triethylamine in THF solution, and di-*tert*-butyl dicarbonate ester (2.18 g, 10 mmol) in methanol solution 6 mL was stirred for 12 h at 25 °C. After reaction completion, the reaction mixture was concentrated under vacuum to give a yellow oily residue, which was further purified with $CHCl_3$ and Na_2CO_3 solution as the extraction solvent to obtain compound **a**. ^{1}H NMR (300 MHz, chloroform-*d*): δ 3.24−3.10 (m, 6H), 2.71 (t, *J* = 6.9 Hz, 2H), 1.45 (s, 9H).

Synthesis of Compound ***b***. A mixture of the respective amino acid (30 mmol) (including L-tryptophan, L-cysteine, L-lysine, and L-glutamic) and di-*tert*-butyl dicarbonate ester (150 mmol) (in a 1:5 molar ratio) in the solvents 15 mL 10% NaOH and 25 mL THF (v/v = 3:5) was stirred at 0 °C for 10 min. Then the reaction mixture was stirred at room temperature for 24 h. After completion, the reaction mixture was concentrated under vacuum to give an oily residue, which was further purified by silica gel column chromatography to obtain compound **b**. ^{1}H NMR (300 MHz, chloroform-*d*): δ 4.05 (q, *J* = 7.1 Hz, 2H), 3.05 (s, 2H), 1.98 (s, 2H), 1.70 (dd, *J* = 45.5, 14.1 Hz, 2H), 1.38 (s, 18H).

Synthesis of Compound ***c***. The compound **b** (1.8 g, 4.95 mmol) was dissolved in a trace of dichloromethane and DCC/NHS (in a 1:1 molar ratio), and the mixture was stirred at 0 °C for 15 min. Compound **a** (0.8 g, 5 mmol) was then added at 0 °C. The reaction mixture was stirred at 25 °C for 16 h. After completion, the reaction mixture was concentrated under vacuum to give a residue, which was further purified by silica gel column chromatography to obtain compound **c**; ^{1}H NMR (300 MHz, chloroform-*d*): δ 4.86 (s, 4H), 4.01 (d, *J* = 7.0 Hz, 2H), 3.27−3.10 (m, 4H), 3.04 (d, *J* = 5.5 Hz, 6H), 1.37 (d, *J* = 1.6 Hz, 27H).

Synthesis of Compound ***d***. The compound **c** (0.75 g, 2 mmol) was dissolved in 2 mL of ethanol solution at 0 °C. Then 6 mL 4 M hydrochloric acid ethanol solution was added at 0 °C. The reaction mixture was stirred at 25 °C for 24 h. After completion, the reaction mixture was concentrated under vacuum to give a solid compound amino-polyamine derivative **d**. ^{1}H NMR (300 MHz, deuterium oxide): δ 3.92 (tt, *J* = 6.6, 2.5 Hz, 1H), 3.22 (q, *J* = 6.2, 5.2 Hz, 2H), 2.94 (td, *J* = 7.4, 3.8 Hz, 4H), 2.00−1.26 (m, 10H). ^{13}C NMR (75 MHz, deuterium oxide): δ 169.49, 53.13, 39.07 (d, *J* = 4.1 Hz), 38.88, 30.38, 26.35, 25.36, 24.22, 21.38.

Synthesis of Compound ***e***. *N*-(3-Dimethylaminopropyl)-3-ethylcarbodiimide hydrochloride (EDC) (7 mg, 0.035 mmol) and NHS (10.5 mg, 0.0875 mmol) were added to AuNP@MPA solution in MES (50 mM, pH 6.5). The reaction mixture was stirred at 25 °C for 30 min. Subsequently, compound **d** (10.5 mg, 0.045 mmol) was added and the mixture was stirred at 25 °C for 24 h. After completion, the reaction mixture was centrifuged to obtain compound **e** (AuNPs@MPA-R-4C).

Synthesis of BODIPY-SO_2Cl. *Synthesis of Compound* ***A***. The *N*-methylpyrrole-2-carboxaldehyde (360 mg, 2.93 mmol) was added to pyrrole solution (400 mg, 2.66 mmol) in CH_2Cl_2 (20 mL). Subsequently, $POCl_3$ (0.4 mL, 2.93 mmol) was added in the above mixed solution dropwise at 0 °C. The mixture was stirred at 25 °C for 6 h and a mixture solution containing compound **A** was obtained.

Synthesis of Compound ***B***. Boron trifluoride etherate ($BF_3{\cdot}OEt_2$, 1.31 mL, 10.6 mmol) and *N*,*N*-diisopropylethylamine (1.9 mL, 11.2 mmol) were added in the mixture solution including compound **A**, and the reaction was stirred at 25 °C for 12 h. The mixture was diluted in a mixture of H_2O (15 mL) and CH_2Cl_2 (10 mL) to filter. The filter paper was washed with CH_2Cl_2 (25 mL) and the organic phases were collected. The organic phases were then dried with Na_2SO_4 under vacuum to give a dark red crude solid residue, and the residue was subjected to column chromatography using 2−7% EtOAc/petroleum ether mixture as the eluent to yield the red oil-shaped compound **B**. ^{1}H NMR (300 MHz, chloroform-*d*): δ 4.32−4.18 (m, 1H), 4.10 (p, *J* = 8.0 Hz, 2H), 1.35 (dt, *J* = 19.7, 7.2 Hz, 5H).

Synthesis of Compound ***C***. Compound **B** (100 mg, 0.4 mmol) in 5 mL dry dichloromethane (CH_2Cl_2) was added with chlorosulfonic acid (4.7 mg, 0.4 mmol) in 2 mL CH_2Cl_2

DOI: 10.1021/acsomega.9b02579
ACS Omega 2019, 4, 17850−17856

dropwise with vigorous stirring at −20 °C. After 0.5 h, the CH_2Cl_2 layer was removed by decanting, and the precipitated thick orange liquid was washed a few times with CH_2Cl_2 to yield compound **C**.

*Synthesis of Compound **D***. The compound **C** (0.49 mmol) in 1 mL acetone and TCT (0.09 g, 0.49 mmol) were added in triethylamine (NEt_3) (0.07 mL, 0.49 mmol), and the reaction was refluxed for 20 h. Subsequently, the reaction mixture was precipitated to give compound **D** (Scheme S1). ^{1}H NMR (300 MHz, DMSO-d_6): δ 4.76 (s, 1H), 3.09 (t, J = 6.1 Hz, 2H), 2.28 (s, 1H), 1.17 (t, J = 7.2 Hz, 4H).

Synthesis of AuNP@MPA-R-4C-X. FITC (1 mg) or BODIPY-SO_2Cl (9 mg) in 200 μL anhydrous dimethylformamide was added with compound **e** in ultrapure water, and the mixture solution was stirred at room temperature for 24 h.[36,39] After completion, the reaction mixture was centrifuged to yield the amino-polyamine derivative-modified AuNPs AuNP@MPA-R-4C-X (Scheme 1c).

Cell Culture. HepG2 (human hepatocellular liver carcinoma), QSG-7701 (human normal liver), and MCF-7 (human breast cancer) cells were maintained in RMPI-1640 medium supplemented with heat-inactivated FBS (10% v/v) and 1% (v/v) penicillin−streptomycin (100 U mL^{-1} penicillin G and 100 mg mL^{-1} streptomycin) at 37 °C under 5% CO_2. These cells were allowed to grow in a monolayer in a tissue culture flask.

Cell Viability Assays. The cell viability of complexes was evaluated in HepG2, QSG-7701, and MCF-7 cells. Briefly, cells were seeded into 96-well plates at 5 × 10^4 cells per well. After 12 h, various concentrations (0.05, 0.10, 0.20, 0.50, and 1.00 mg/mL) of samples were subsequently added and incubated for 48 h (the concentration of original AuNPs was 0.001, 0.005, 0.01, 0.02, and 0.05 mg/mL). Then 20 μL 3-(4,5-dimethyl-2-thiazolyl)-2,5-diphenyltetrazolium bromide (MTT) (2.5 mg/mL) was added to each well. After 4 h incubation, the medium was then removed and 100 mL DMSO was added to the plates to dissolve the formazan products. The absorbance of the solution containing the extracts was read at 570 nm on a Tecan Infinite F200 M200 multimode plate reader. The inhibition rate was calculated from the plotted results using untreated cells as 100%.

Cellular Uptake of Targeted AuNP@MPA-R-4C-X. Cells seeded in a 6-well tissue culture plate (Corning) were incubated with AuNP@MPA-R-4C-FITC or AuNP@MPA-R-4C-BODIPY with a different concentration and different incubation time at 37 °C. After incubation for indicated time points, the cells were thoroughly washed with phosphate-buffered saline buffer at pH 7.4, and incubated with Hoechst 33342 (10 mg/mL) or WGA, Alexa Flour 594 (5 μg/mL) for 30 min at 37 °C, and then viewed with a confocal microscope (Leica-SP8). The nucleus and cell membrane were obtained by counting in eight randomly chosen fields per dish per experimental group from three separate experiments. Cell nuclei stained with Hoechst 33342 were observed under an emission at 405 nm and analyzed from 430 to 480 nm. In addition the membrane stained with AuNP@MPA-R-4C-BODIPY was observed under an emission at 590 nm and analyzed from 615 to 635 nm. AuNP@MPA-R-4C-FITC was excited at 488 nm with an Ar laser. A band pass from 500 to 560 nm was used for observation.

TEM Analysis. Cells incubated with samples were first fixed in 2.5% glutaraldehyde (in 0.1 M phosphate buffer, pH 7.0). The cells were fixed with 1% perosmic oxide for 2 h at 4 °C. After being washed in water, the cells were dehydrated in a series of alcohol, embedded, and sliced with the thickness between 50 and 70 nm. TEM analysis was performed on a JEM-1230EX transmission electron microscope operating at 80 kV in bright field mode.

■ ASSOCIATED CONTENT

Supporting Information

The Supporting Information is available free of charge on the ACS Publications website at DOI: 10.1021/acsomega.9b02579.

Schematic illustration of the synthesis of BODIPY-SO_2Cl, TEM images, DLS particle size distributions, UV−vis absorption spectra, fluorescence spectra, and confocal images of HepG2 cells treated with FITC (PDF)

■ AUTHOR INFORMATION

Corresponding Author

*E-mail: zhaomeixia2011@henu.edu.cn.

ORCID

Chaojie Wang: 0000-0001-6782-0650

Mei-Xia Zhao: 0000-0002-2635-788X

Notes

The authors declare no competing financial interest.

■ ACKNOWLEDGMENTS

This work was supported by the National Natural Science Foundation of China (21501044), Program for Innovative Research Talents from the University of Henan Province (18HASTIT049), Foundation of Science and Technology Department of Henan Province (182102410075), First-class discipline cultivation project of Henan University-innovation team cultivation, and Special Professor project of Henan University.

■ REFERENCES

(1) Bethany, A. W.; Robert, C. O.; Alyssa, J.; Gregory, W. C.; Neal, M. A. A Systematic Exploration of the Interactions between Bacterial Effector Proteins and Host Cell Membranes. *Nat. Commun.* **2017**, *8*, 532.

(2) Zhao, M.-X.; Zhu, B.-J. The Research and Applications of Quantum Dots as Nano-Carriers for Targeted Drug Delivery and Cancer Therapy. *Nanoscale Res. Lett.* **2016**, *11*, 207.

(3) Phillips, M. C.; Johnson, W. J.; Rothblat, G. H. Mechanisms and Consequences of Cellular Cholesterol Exchange and Transfer. *Biochim. Biophys. Acta.* **1987**, *906*, 223−276.

(4) Kim, J. H.; Ren, Y.; Ng, W. P.; Li, S.; Son, S.; Kee, Y.-S.; Zhang, S.; Zhang, G.; Fletcher, D. A.; Robinson, D. N.; Chen, E. H. Mechanical Tension Drives Cell Membrane Fusion. *Dev. Cell* **2015**, *32*, 561−573.

(5) Saurel, O.; Iordanov, I.; Nars, G.; Demange, P.; Le Marchand, T.; Andreas, L. B.; Pintacuda, G.; Milon, A. Local and Global Dynamics inKlebsiella pneumoniaeOuter Membrane Protein a in Lipid Bilayers Probed at Atomic Resolution. *J. Am. Chem. Soc.* **2017**, *139*, 1590−1597.

(6) Abadeer, N. S.; Murphy, C. J. Recent Progress in Cancer Thermal Therapy Using Gold Nanoparticles. *J. Phys. Chem. C* **2016**, *120*, 4691−4716.

(7) Zhao, M.-X.; Zeng, E.-Z. Application of Functional Quantum Dot Nanoparticles as Fluorescence Probes in Cell Labeling and Tumor Diagnostic Imaging. *Nanoscale Res. Lett.* **2015**, *10*, 171.

DOI: 10.1021/acsomega.9b02579
ACS Omega 2019, 4, 17850−17856

(8) Ali, M. R. K.; Wu, Y.; El-Sayed, M. A. Gold-Nanoparticle-Assisted Plasmonic Photothermal Therapy Advances Toward Clinical Application. *J. Phys. Chem. C* **2019**, *123*, 15375−15393.
(9) Cabuzu, D.; Cirja, A.; Puiu, R.; Grumezescu, A. Biomedical Applications of Gold Nanoparticles. *Curr. Top. Med. Chem.* **2015**, *15*, 1605−1613.
(10) Liu, Y.; Liu, M.; Swihart, M. T. Plasmonic Copper Sulfide-Based Materials: A Brief Introduction to Their Synthesis, Doping, Alloying, and Applications. *J. Phys. Chem. C* **2017**, *121*, 13435−13447.
(11) Zhao, M.-X.; Zeng, E.-Z.; Zhu, B.-J. The Biological Applications of Inorganic Nanoparticle Drug Carriers. *ChemNanoMat* **2015**, *1*, 82−91.
(12) Han, G.; Ghosh, P.; Rotello, V. M. Multi-functional Gold Nanoparticles for Drug Delivery. *Adv. Exp. Med. Biol.* **2007**, *620*, 48−56.
(13) Chen, D.; Wang, G.; Li, J. Interfacial Bioelectrochemistry: Fabrication, Properties and Applications of Functional Nanostructured Biointerfaces. *J. Phys. Chem. C* **2007**, *111*, 2351−2367.
(14) Khristosov, M. K.; Bloch, L.; Burghammer, M.; Kauffmann, Y.; Katsman, A.; Pokroy, B. Sponge-like Nanoporous Single Crystals of Gold. *Nat. Commun.* **2015**, *6*, 8841.
(15) Alba-Molina, D.; Santiago, A. R. P.; Giner-Casares, J. J.; Martín-Romero, M. T.; Camacho, L.; Luque, R.; Cano, M. Citrate-Stabilized Gold Nanoparticles as High-Performance Electrocatalysts: The Role of Size in the Electroreduction of Oxygen. *J. Phys. Chem. C* **2019**, *123*, 9807−9812.
(16) Korotcenkov, G.; Brinzari, V.; Cho, B. K. Conductometric Gas Sensors Based on Metal Oxides Modified with Gold Nanoparticles: A Review. *Microchim. Acta* **2016**, *183*, 1033−1054.
(17) Ali, M. R. K.; Wu, Y.; El-Sayed, M. A. Gold-Nanoparticle-Assisted Plasmonic Photothermal Therapy Advances Toward Clinical Application. *J. Phys. Chem. C* **2019**, *123*, 15375−15393.
(18) Zhao, M.-X.; Cai, Z.-C.; Zhu, B.-J.; Zhang, Z.-Q. The Apoptosis Effect on Liver Cancer Cells of Gold Nanoparticles Modified with Lithocholic Acid. *Nanoscale Res. Lett.* **2018**, *13*, 304.
(19) Paulo, P. M. R.; Botequim, D.; Jóskowiak, A.; Martins, S.; Prazeres, D. M. F.; Zijlstra, P.; Costa, S. M. B. Enhanced Fluorescence of a Dye on DNA-Assembled Gold Nanodimers Discriminated by Lifetime Correlation Spectroscopy. *J. Phys. Chem. C* **2018**, *122*, 10971−10980.
(20) Jeong, E. H.; Jung, G.; Hong, C. A.; Lee, H. Gold Nanoparticle (AuNP)-Based Drug Delivery and Molecular Imaging for Biomedical Applications. *Arch. Pharm. Res.* **2014**, *37*, 53−59.
(21) Guirgis, B. S. S.; Sá e Cunha, C.; Gomes, I.; Cavadas, M.; Silva, I.; Doria, G.; Blatch, G. L.; Baptista, P. V.; Pereira, E.; Azzazy, H. M. E.; Mota, M. M.; Prudêncio, M.; Franco, R. Gold Nanoparticle-Based Fluorescence Immunoassay for Malaria Antigen Detection. *Anal. Bioanal. Chem.* **2012**, *402*, 1019−1027.
(22) Bodelón, G.; Costas, C.; Pérez-Juste, J.; Pastoriza-Santos, I.; Liz-Marzán, L. M. Gold Nanoparticles for Regulation of Cell Function and Behavior. *Nano Today* **2017**, *13*, 40−60.
(23) Huang, H.; Li, H.; Feng, J.-J.; Wang, A.-J. Peptide-Directed Synthesis of Fluorescent Gold Nanoparticles for Mitochondria-Targeted Confocal Imaging of Temperature. *Microchim. Acta* **2017**, *184*, 1215−1221.
(24) Muroski, M. E.; Morgan, T. J.; Levenson, C. W.; Strouse, G. F. A Gold Nanoparticle Pentapeptide: Gene Fusion To Induce Therapeutic Gene Expression in Mesenchymal Stem Cells. *J. Am. Chem. Soc.* **2014**, *136*, 14763−14771.
(25) Hunkapiller, M. W.; Lujan, E.; Ostrander, F.; Hood, L. E. Isolation of microgram quantities of proteins from polyacrylamide gels for amino acid sequence analysis. *Methods Enzymol.* **1983**, *91*, 227−236.
(26) Hansen, J. C.; Lu, X.; Ross, E. D.; Woody, R. W. Intrinsic Protein Disorder, Amino Acid Composition, and Histone Terminal Domains. *J. Biol. Chem.* **2006**, *281*, 1853−1856.
(27) Purwaha, P.; Lorenzi, P. L.; Silva, L. P.; Hawke, D. H.; Weinstein, J. N. Targeted Metabolomic Analysis of Amino Acid Response to L-Asparaginase in Adherent Cells. *Metabolomics* **2014**, *10*, 909−919.
(28) Rajendran, E.; Rajendran, E.; Hapuarachchi, S. V.; Miller, C. M.; Fairweather, S. J.; Cai, Y.; Smith, N. C.; Cockburn, I. A.; Bröer, S.; Kirk, K.; van Dooren, G. G. Cationic Amino Acid Transporters Play Key Roles in the Survival and Transmission of Apicomplexan Parasites. *Nat. Commun.* **2017**, *8*, 14455.
(29) Mayilo, S.; Kloster, M. A.; Wunderlich, M.; Lutich, A.; Klar, T. A.; Nichtl, A.; Kürzinger, K.; Stefani, F. D.; Feldmann, J. Long-Range Fluorescence Quenching by Gold Nanoparticles in a Sandwich Immunoassay for Cardiac Troponin T. *Nano Lett.* **2009**, *9*, 4558−4563.
(30) Hall, A. Rho GTPases and the Actin Cytoskeleton. *Science* **1998**, *279*, 509−514.
(31) Raza, M. K.; Gautam, S.; Garai, A.; Mitra, K.; Kondaiah, P.; Chakravarty, A. R. Monofunctional BODIPY-Appended Imidazoplatin for Cellular Imaging and Mitochondria-Targeted Photocytotoxicity. *Inorg. Chem.* **2017**, *56*, 11019−11029.
(32) Mu, L.; Feng, S. S. Vitamin E TPGS Used as Emulsifier in the Solvent Evaporation/Extraction Technique for Fabrication of Polymeric Nanospheres for Controlled Release of Paclitaxel (Taxol). *J. Control. Release* **2002**, *80*, 129−144.
(33) Zhao, M.-X.; Li, J.-M.; Du, L.; Tan, C.-P.; Xia, Q.; Mao, Z.-W.; Ji, L.-N. Targeted Cellular Uptake and siRNA Silencing by Quantum-Dot Nanoparticles Coated with β-Cyclodextrin Coupled to Amino Acids. *Chem.—Eur. J.* **2011**, *17*, 5171−5179.
(34) Wang, X.; Guo, L.; Zhang, S.; Chen, Y.; Chen, Y.-T.; Zheng, B.; Sun, J.; Qian, Y.; Chen, Y.; Yan, B.; Lu, W. Copper Sulfide Facilitates Hepatobiliary Clearance of Gold Nanoparticles through the Copper-Transporting ATPase ATP7B. *ACS Nano* **2019**, *13*, 5720−5730.
(35) Wang, Y.; Chen, G.; Yang, M.; Silber, G.; Xing, S.; Tan, L. H.; Wang, F.; Feng, Y.; Liu, X.; Li, S.; Chen, H. A Systems Approach towards the Stoichiometry-Controlled Hetero-Assembly of Nanoparticles. *Nat. Commun.* **2010**, *1*, 87.
(36) Steinbach, J. M.; Seo, Y.-E.; Saltzman, W. M. Cell Penetrating Peptide-Modified Poly(lactic-co-glycolic acid) Nanoparticles with Enhanced Cell Internalization. *Acta Biomater.* **2016**, *30*, 49−61.
(37) Wang, G.; Stender, A. S.; Sun, W.; Fang, N. Optical Imaging of Non-Fluorescent Nanoparticle Probes in Live Cells. *Analyst* **2010**, *135*, 215−221.
(38) Turkevich, J.; Stevenson, C. P.; Hillier, J. A Study of the Nucleation and Growth Processes in the Synthesis of Colloidal Gold. *Discuss. Faraday Soc.* **1951**, *11*, 55−75.
(39) Schneider, G.; Decher, G.; Nerambourg, N.; Praho, R.; Werts, M. H.; Blanchard-Desce, M. Distance-Dependent Fluorescence Quenching on Gold Nanoparticles Ensheathed with Layer-by-Layer Assembled Polyelectrolytes. *Nano Lett.* **2006**, *6*, 530−536.

DOI: 10.1021/acsomega.9b02579
ACS Omega 2019, 4, 17850−17856